AD

BRL

TECHNICAL REPORT ARBRL-TR-02047

(Supersedes IMR No. 548)

STRUCTURAL RESPONSE INDUCED BY ELECTRON BEAM DEPOSITION

Norris J. Huffington, Jr.
Henry L. Wisniewski

March 1978

DDC
RECEIVED
APR 7 1978
B

USA ARMAMENT RESEARCH AND DEVELOPMENT COMMAND
USA BALLISTIC RESEARCH LABORATORY
ABERDEEN PROVING GROUND, MARYLAND

REPORT DOCUMENTATION PAGE		READ INSTRUCTIONS BEFORE COMPLETING FORM
1. REPORT NUMBER TECHNICAL REPORT ARBRL-TR-02047	2. GOVT ACCESSION NO.	3. RECIPIENT'S CATALOG NUMBER
4. TITLE (and Subtitle) STRUCTURAL RESPONSE INDUCED BY ELECTRON BEAM DEPOSITION.		5. TYPE OF REPORT & PERIOD COVERED Final rept.
		6. PERFORMING ORG. REPORT NUMBER
7. AUTHOR(s) Norris J. Huffington, Jr. Henry L. Wisniewski		8. CONTRACT OR GRANT NUMBER(s) 34p.
9. PERFORMING ORGANIZATION NAME AND ADDRESS US Army Ballistic Research Laboratory (ATTN: DRDAR-BLT) Aberdeen Proving Ground, MD 21005		10. PROGRAM ELEMENT, PROJECT, TASK AREA & WORK UNIT NUMBERS RDT&E 1W162118AH75
11. CONTROLLING OFFICE NAME AND ADDRESS US Army Armament Research & Development Command US Army Ballistic Research Laboratory (ATTN: DRDAR-BL) Aberdeen Proving Ground, MD 21005		12. REPORT DATE MAR 78
		13. NUMBER OF PAGES 45
14. MONITORING AGENCY NAME & ADDRESS(if different from Controlling Office)		15. SECURITY CLASS. (of this report) UNCLASSIFIED
		15a. DECLASSIFICATION/DOWNGRADING SCHEDULE

16. DISTRIBUTION STATEMENT (of this Report)

Approved for public release; distribution unlimited.

17. DISTRIBUTION STATEMENT (of the abstract entered in Block 20, if different from Report)

18. SUPPLEMENTARY NOTES

This report supersedes IMR 548.

19. KEY WORDS (Continue on reverse side if necessary and identify by block number)

Structural Response	X-Ray Deposition
Finite Difference	Cylindrical Shells
Electron Beam	AURORA Facility
Radiation Simulation	

20. ABSTRACT (Continue on reverse side if necessary and identify by block number)

The response of a generic shell structure to electron beam excitation is modeled analytically by use of finite difference codes. Good agreement between model predictions and experimental data for the deformation of a cylindrical shell was obtained for a specific assumed circumferential variation of electron beam fluence. Consideration is given to the potential of a large scale electron beam facility to serve as a simulator for x-ray loading of structures.

393 471

DD FORM 1473 1 JAN 73   EDITION OF 1 NOV 65 IS OBSOLETE

TABLE OF CONTENTS

LIST OF ILLUSTRATIONS

I. INTRODUCTION

The feasibility of modeling the response of a generic structure excited by electron beam energy deposition and of correlating the results with available test data was undertaken by the Ballistic Research Laboratory at the request of the Harry Diamond Laboratories. Success in this endeavor would enhance the basis for utilization of a large-scale electron beam facility for simulation of the effects of intense x-rays on missile and re-entry vehicle structures, thus reducing the requirement for costly and time-consuming underground nuclear tests.

Experimental data were obtained for aluminum alloy cylinders of various wall thicknesses by HDL personnel using the AURORA facility in the electron beam mode. These cylinders had thin lead overlays selected so as to absorb sufficient energy from the electron beam to be partially melted or vaporized and to impart an impulse to the aluminum cylinders as they were blown away. Films made with a high speed framing camera showed that this technique was successful. Large deformations were induced in some of the aluminum cylinders. Many of these structural cylinders were instrumented on the inside with strain gages to record transient strains at various positions around the circumference.

The modeling aspect of this investigation has similarities to a previously reported BRL study[1,2], the principal differences being that the earlier work was concerned with x-ray, rather than electron beam, deposition and the previous structural configuration was an initially flat plate. In the following sections of this report necessary details of the AURORA tests will be provided, the procedures followed in modeling this experiment will be discussed, and the correlation between predictions and test data will be evaluated.

II. THE EXPERIMENTAL CONFIGURATION

The structural cylinders each had an outside diameter of 152.4 mm (6.0 inches) and were fabricated from 6061-T6 aluminum alloy by rolling and butt welding. The stress-strain diagram obtained by pulling a tensile specimen of this material is shown in Figure 1. These cylinders were 190.5 mm (7.5 inches) long and were supported at the ends

---

[1] N. J. Huffington, Jr. and H. L. Wisniewski, "Structural Response Induced by X-Rays," Proceedings of the Fifth Symposium on Nuclear Survivability of Propulsion and Ordnance Systems, October 1975.

[2] H. L. Wisniewski, "Coupling of X-Ray Deposition to Structural Response," U.S. Army Ballistic Research Laboratories Memorandum Report No. 2761, June 1977. (AD #A042667)
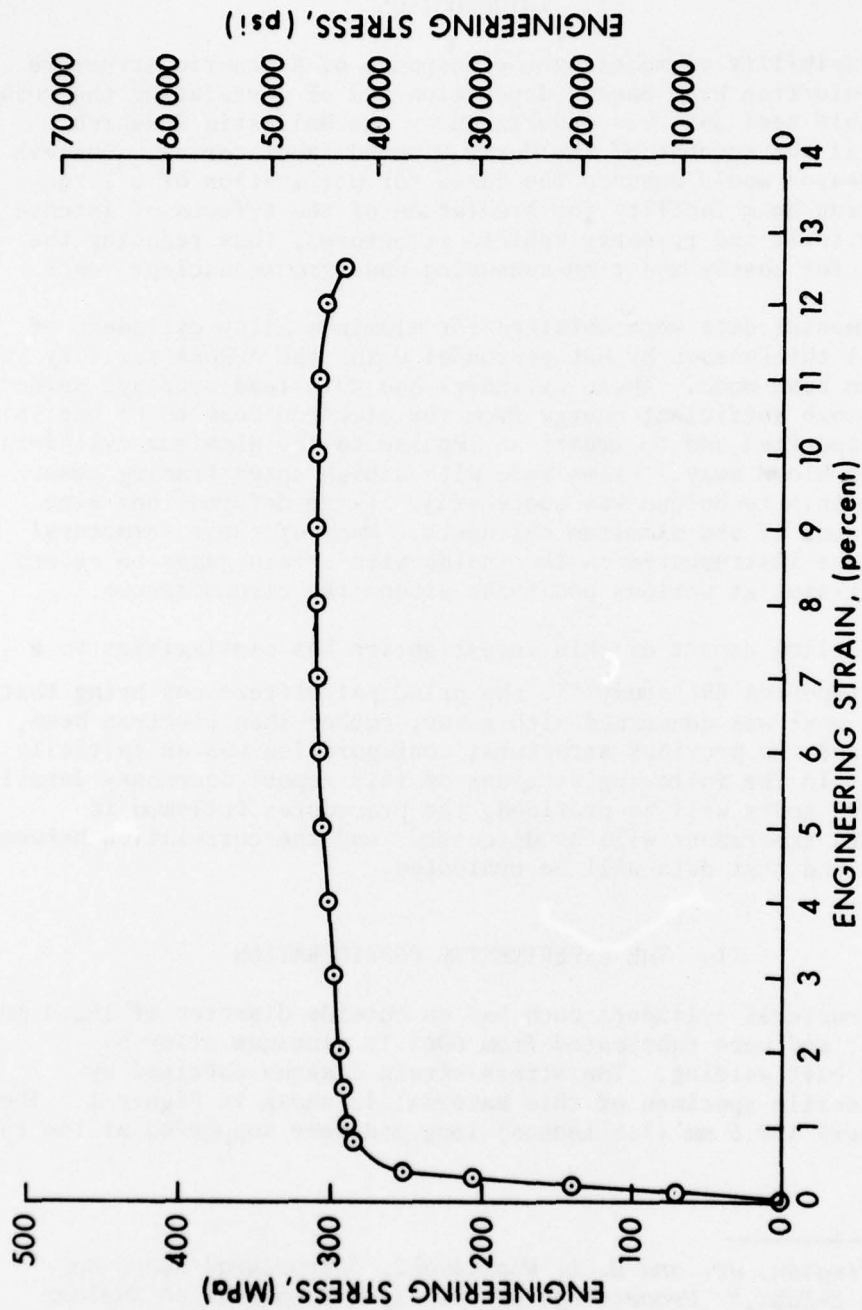
Figure 1. Tensile Stress-Strain Curve for 6061-T6 Aluminum Alloy Sheet used for Cylinder Specimen

by stepped discs as shown in Figure 2. In turn, these discs are presumed to be rigidily secured to an immovable foundation during the test. The free length of the cylinders between the end discs was 152.4 mm (6.0 inches); however, since the same end fittings were used regardless of the gauge of the cylinders, it is presumed that there was some "slop" between cylinder and end discs for the thinner gauge cylinders. This poses a problem as to the proper modeling of boundary conditions for the cylinders in the response analysis.

Rather than consider a spectrum of test data, the succeeding discussion will consider only a single representative test (Pulse 1772), for which the aluminum cylinder had a gauge of 1.549 mm (0.061 inches) and the lead overlay was 1.727 mm (0.068 inches) in thickness. As shown in Figure 2, the specimen was positioned so that the axis of the electron beam was perpendicular to the axis of the cylinder and passed through it. In future references to circumferential locations, the angle θ will be measured from the direction of the incident electron beam, as indicated. Foil type strain gages were cemented to the inside of the cylinder at angles 0°, 90°, 180°, and 270°, midway between the ends of the cylinder

Figure 2. Cylinder Test Configuration

9

with their axes oriented in the longitudinal direction. The splice in the aluminum cylinder was located at $\theta = 145°$ while the splice in the lead overlay was also positioned on the back side of the cylinder within $20°$ from $\theta = 180°$.

This target configuration was subjected to a pulsed 8 MeV mono-energetic electron beam with a fluence of 60 cal/cm^2 in the drift tube of the AURORA facility. Figure 3 is a post-test photograph of the aluminum cylinder which shows the extent of permanent deformation induced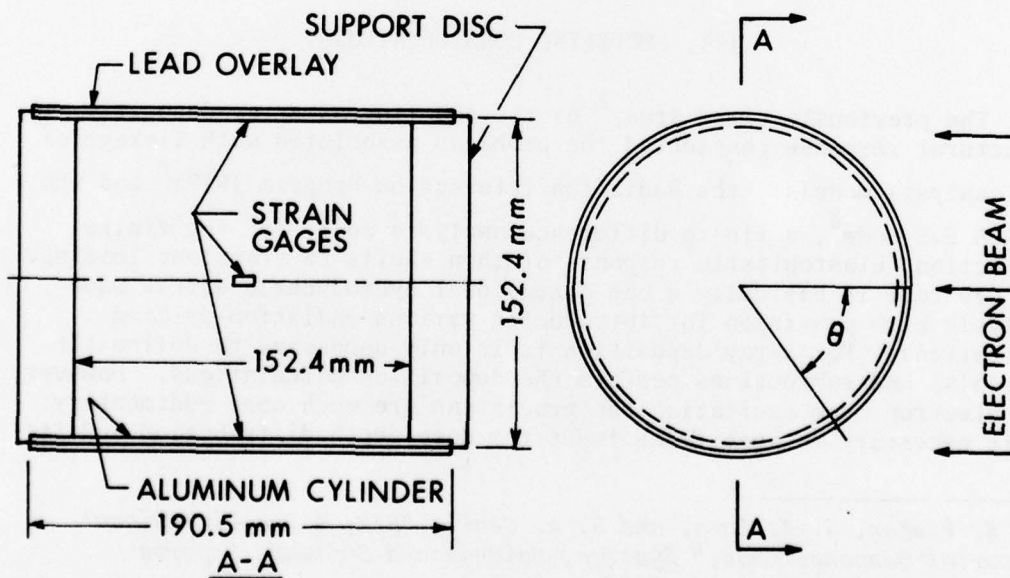 in this specimen. Quantitative measurements of the deformed cylinder will be presented when comparisons are made with predictions. Figure 4 is a photograph of the recovered soft lead overlay in a flattened position. On the average, 366 mm (14.4 inches) of the length of this strip (corresponding to a circumferential angle of 272°) was visibly unaffected by the electron beam. The remaining 88° of the circumference of the lead cylinder was partially melted or blown off. At each end of the residual lead overlay there is a region of tapering thickness approximately 64 mm (2.5 inches) wide which has undergone metallurgical transition. Since the total length of the lead strip is appreciably greater than the initial circumference of the lead overlay, the affected region must have stretched like taffy before rupturing. There is no evidence that the electron beam impinged directly upon the aluminum cylinder.

III. MODELING CONSIDERATIONS

The previously cited study[2] of the coupling of x-ray deposition to structural response considered the problems associated with linkage of two analysis models: the Radiation Interaction Program (RIP)[3] and the PETROS 3.5 code[4], a finite difference analysis model for the finite deflection, elastoplastic response of thin shells to transient loading. The RIP code is basically a one-dimensional hydrodynamic stress wave analysis with provision for introducing various radiation-related excitations. For x-ray deposition it is only necessary to define the source(s) and subroutines perform the deposition calculations. However, for electron beam excitation the provisions are much more rudimentary: it is necessary to specify as input the dose-depth distribution and its

---

[3] R. H. Fisher, G. A. Lane, and R. A. Cecil, "RIP, A One-Dimensional Material Response Code," Systems, Science and Software Reports 3SR-751-I & II, September 1972.

[4] S. D. Pirotin, B. A. Berg, and E. A. Witmer, "PETROS 3.5: New Developments and Program Manual for the Finite-Difference Calculation of Large Elastic-Plastic Transient Deformations of Multilayer Variable-Thickness Shells," U.S. Army Ballistic Research Laboratories Contract Report No. 211, February 1975. (AD #A007215)
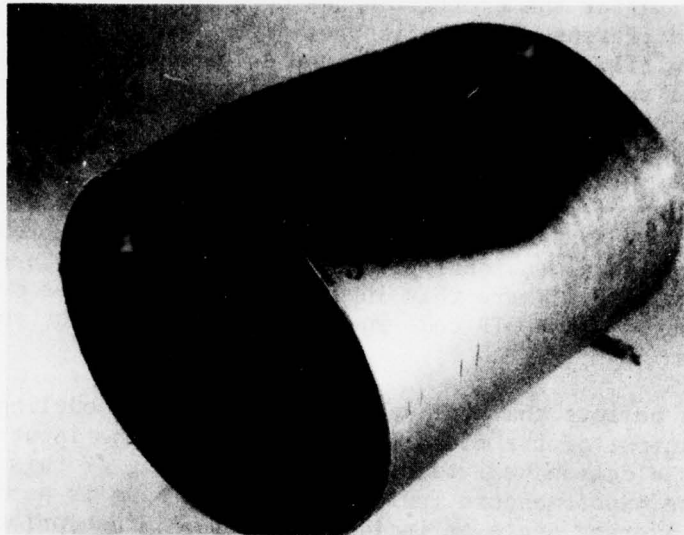
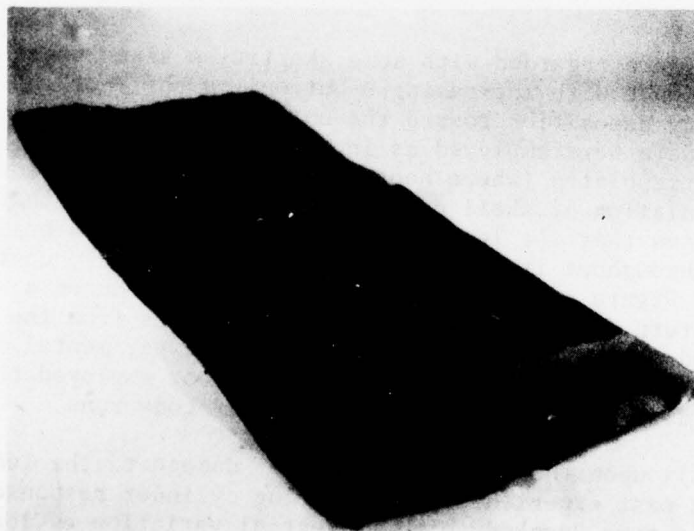Figure 3. Cylinder Deformation Induced by Electron Beam

Figure 4. Post-Test Photograph of Lead Overlay

time dependence. After the excitation has been defined the RIP code performs finite difference calculations of stress wave propagation and reflections in multilayer plates. When the solution has been marched out in time for a sufficient period, information may be extracted from the RIP code concerning mean velocities acquired by the structure, inelastic stress states established by the passage of intense stress waves, and temperature distributions (which may be sufficiently high that thermal degradation of material properties must be considered) for introduction into the PETROS 3.5 code. These data are required for each mesh point of the two-dimensional grid defining the reference surface of the shell structure. Where this input information varies over the surface of the shell, many RIP code runs may be required for an adequate definition.

The authors believe that the weakest link in this modeling chain is between the output of the field emission tube and the input to the RIP code for its electron beam mode. At the beginning of this investigation the experimenters indicated that the beam is perfectly uniform with an average angle of incidence of 45°. Since prior experience with shell response codes had demonstrated that the response pattern of the cylinder would be quite sensitive to the distribution of surface loading, more specific deposition information was requested. We were then provided with predictions of dose-depth distribution obtained from runs with the one-dimensional electron transport code ZEBRA[5] for each 15° of circumferential angle of the front side of the cylinder (see Figure 5).

These data were regarded with some skepticism since there was no reduction of fluence with increasing θ but only a shift of the location of maximum energy deposition toward the outer surface of the lead. However, these data were employed as input for seven RIP runs and the results were interpolated (where necessary) to obtain input for a PETROS 3.5 calculation of shell deformation. It was found that the RIP runs predicted that the lead was either melted or in a solid-spalled state throughout its thickness for $-90° \leq \theta \leq 90°$, contrary to the evidence of Figure 4. Also the PETROS 3.5 run produced a deformation pattern (shown in Figure 6) which differs from the observed in both form and amplitude (see Figure 3 and the experimental contours in Figure 6). It must be concluded that we had not employed the correct energy distribution as input for the RIP code runs.

Based partly upon the observed extent of damage to the lead overlay and partly upon past experience in predicting cylinder response which indicated that a more "peaked" circumferential variation of loading was required to produce the pattern of Figure 3, it was decided to employ

---

[5] L. D. Buxton, "The Electron Transport Computer Code ZEBRA 1," Harry Diamond Laboratories TR-1536, June 1971.
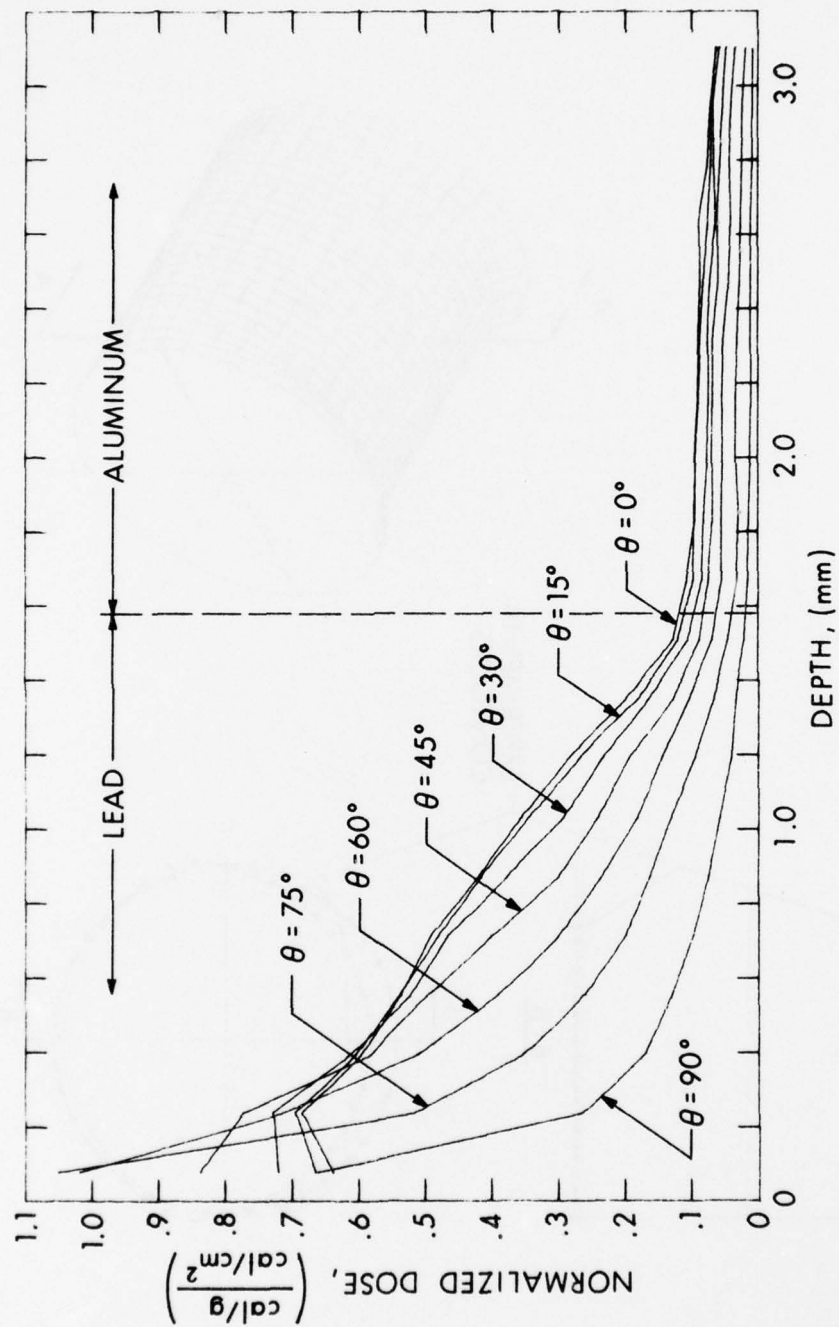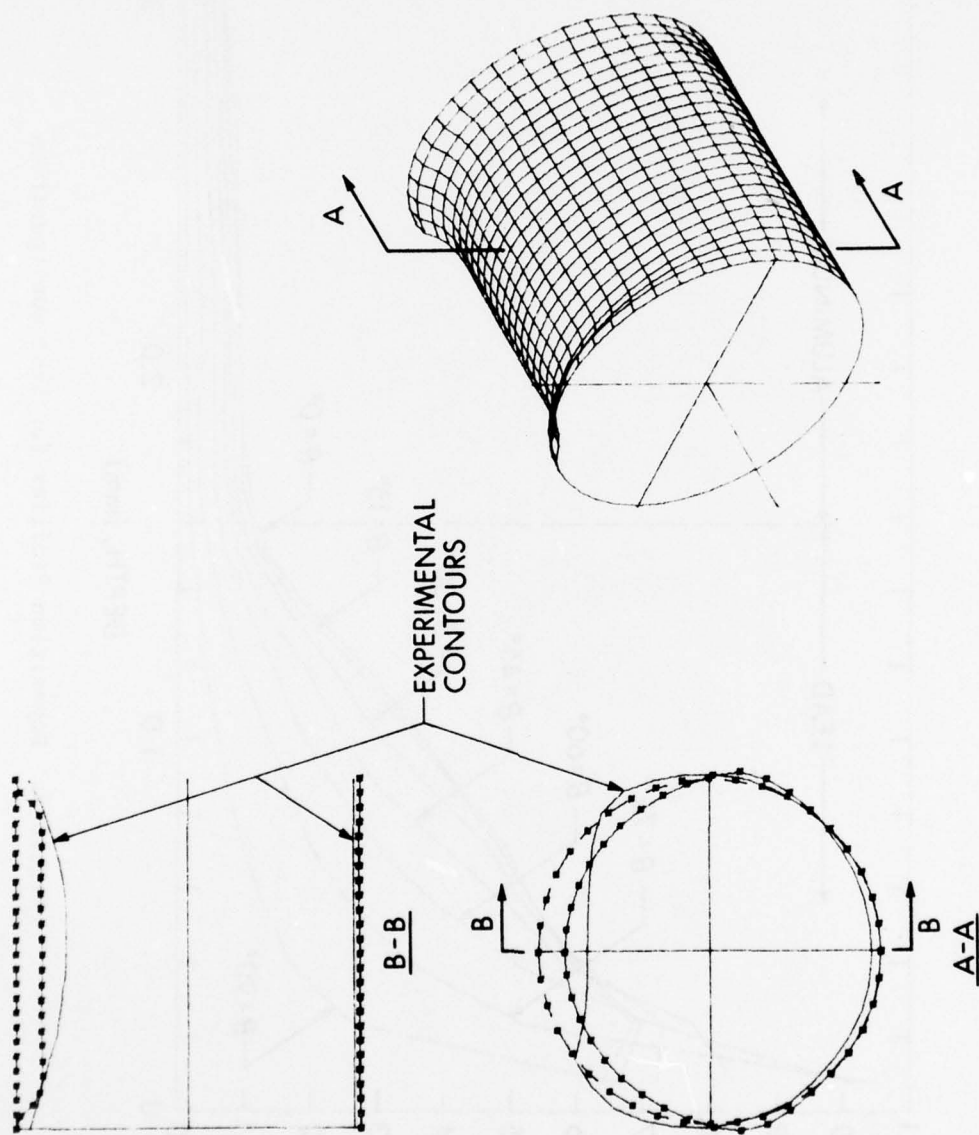
12

Figure 5. Deposition Profiles for Test Configuration

13

EXPERIMENTAL
CONTOURS

B-B

B-A

Figure 6. Preliminary Cylinder Deformation Prediction

14

the dose-depth distribution for $\theta = 0$ but with the 60 cal/cm^2 fluence scaled down according to the function

$$F(\theta) = \begin{cases} \cos 2\theta & \text{for} \quad |\theta| \leqslant 45° \\ \\ 0 & \text{for } 45° < |\theta| \leqslant 180° \end{cases} \tag{1}$$

It will be seen that this results in much better agreement with the available test data.

IV. THEORETICAL/EXPERIMENTAL CORRELATIONS FOR THE IMPROVED RESPONSE MODEL

A. <u>Material Response</u>

The dose-depth distribution resulting from use of Equation (1) is exhibited in Figure 7. RIP code runs using the electron beam mode were made for each of the angles θ shown in this figure. Nine degree intervals were chosen to match the nodal point locations selected for the PETROS 3.5 code calculation to follow. For each RIP code calculation the thickness of the lead overlay was subdivided into 102 cells, while 40 cells were used to represent the thickness of the aluminum cylinder. The GRAY equation of state was employed for both materials, using the properties listed in Tables I and II.

The RIP calculations were performed in the normal undamped manner until the plastic work was essentially complete, at which point damping was introduced to suppress the through-thickness stress waves. This process is illustrated in Figure 8, which shows the variation of the kinetic energy of a longitudinal strip of aluminum at the cited angle (recall that this is a one-dimensional calculation). In this instance damping was initiated slightly after 1.4 µs. The residual kinetic energy is that of uniform radial inward motion. The corresponding variations of the velocities of the mass centers of the aluminum strips at various angles θ obtained from the RIP code runs are depicted in Figure 9. When damping is complete there is no through-thickness motion relative to the mass center and the stresses in this direction have vanished. However, when plastic work has been done there will generally exist residual tangential stresses; i.e., in-plane stresses in the cylindrical shell. Figure 10 shows a representative through-thickness distribution of these residual tangential stresses, which must be transferred as input to the structural response calculation. Also obtained from the RIP code solutions was information on temperature distributions produced by the electron beam deposition, a typical one of which is shown in Figure 11. Since for all angles the aluminum experienced a temperature rise of only a few degrees above ambient (300°K), it may be concluded that it is unnecessary to give further consideration to thermal stresses or thermal degradation of material properties in the response modeling.

15
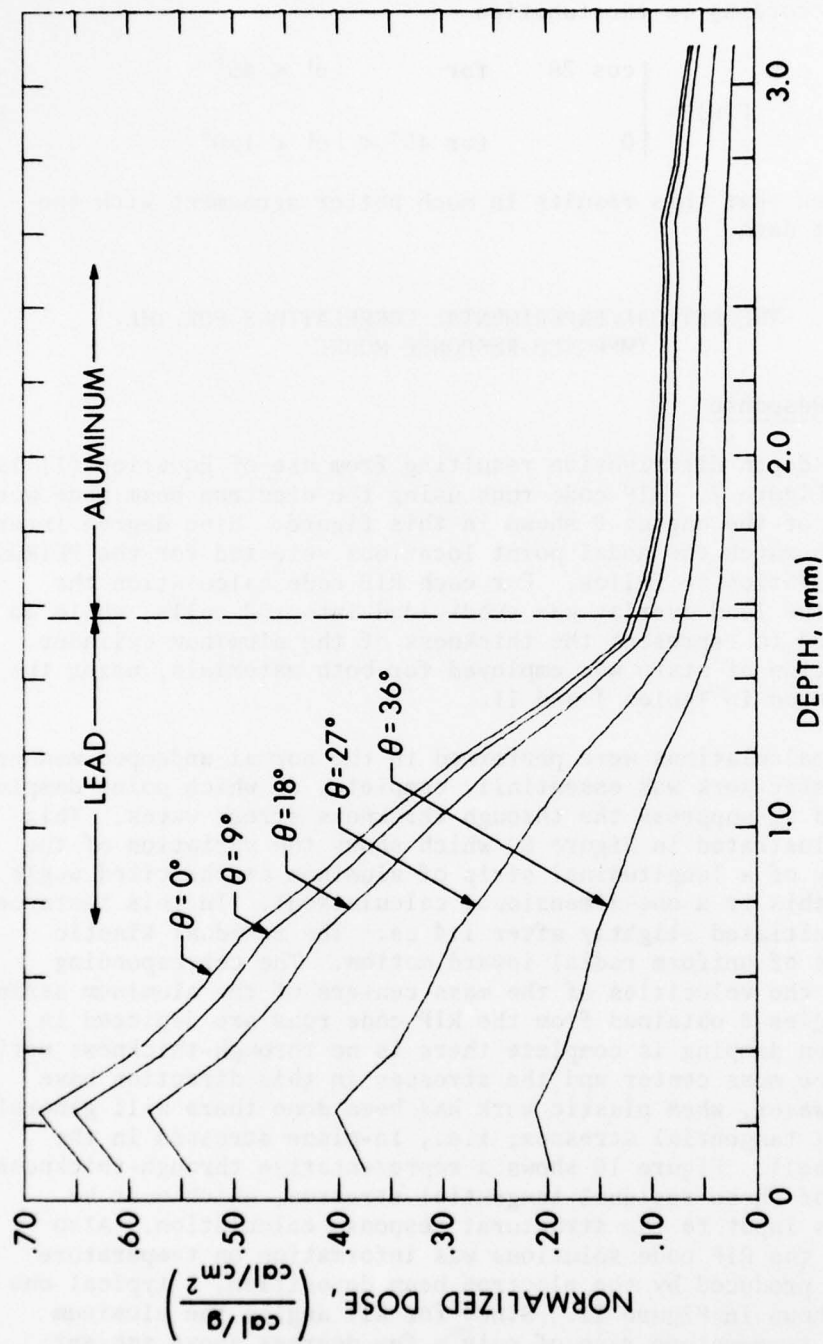
Figure 7. Modified Deposition Profiles

Table I. GRAY Equation of State Parameters for Lead

Symbol	Numerical Value		Property
ρ_o	11.355	gm/cm^2	Ambient density
C_o	2.1×10^5	cm/sec	Bulk sound speed
AMU	5.56×10^{10}	dynes/cm^2	Shear Modulus
Y_o	1.0×10^8	dynes/cm^2	Yield strength
σ_o	-1.0×10^{10}	dynes/cm^2	Spall limit
E_{VV}	9.43×10^9	ergs/cm	Material has vaporized
E_{LV}	2.90×10^9	ergs/cm	Material commences to vaporize
E_{LM}	6.90×10^8	ergs/cm	Material has completed melting
E_{SM}	4.10×10^8	ergs/cm	Material commences to melt
S	1.54		Hugoniot parameter
γ_o	2.84	dimensionless	Lattice gamma
a	2.3		$a = \gamma_o - .5$
γ_e	.6667		Electronic gamma
g_e	14.7×10^{-9}	Mbar-cm^3/mole-deg^2	Electronic energy coefficient
T_{mo}	760.	K	Melting temperature parameter
AW	207.2	gm/mole	Atomic weight
V_J	.109	cm^3/gm	Volume at which EOS are joined
V_b	.042	cm^3/gm	Excluded volume for vapor phase
a_y	49.	Mbar (cm^3/mole)	Coefficient of attractive potential for vapor
θ	1.0	dimensionless	Joint parameter
DELS	9.637×10^{-5}	Mbar-cm^3/mole-deg	Entropy of melting

NOTE: Cgs rather than SI units are listed in Tables I and II since these units are required for the present version of the RIP code.

Table II. GRAY Equation of State Parameters for 6061-T6 Aluminum

Symbol	Numerical Value		Property
ρ_o	2.704	gm/cm^3	Ambient density
C_o	5.21×10^5	cm/sec	Bulk sound speed
AMU	2.79×10^{11}	dynes/cm^2	Shear Modulus
Y_o	2.77×10^9	dynes/cm^2	Yield strength
σ_o	-1.3×10^{10}	dynes/cm^2	Spall limit
E_{VV}	1.2×10^{11}	ergs/cm	Material has vaporized
E_{LV}	3.05×10^{10}	ergs/cm	Material commences to vaporize
E_{LM}	1.1×10^{10}	ergs/cm	Material has completed melting
E_{SM}	7.15×10^9	ergs/cm	Material commences to melt
S	1.338		Hugoniot parameter
γ_o	2.18	dimensionless	Lattice gamma
a	1.68		$a = \gamma_o - .5$
γ_e	.6667		Electronic gamma
g_e	8.7×10^{-9}	Mbar-cm^3/mole-deg^2	Electronic energy coefficient
T_{mo}	1340.	K	Melting temperature parameter
AW	26.98	gm/mole	Atomic weight
V_J	.452	cm^3/gm	Volume at which EOS are joined
V_b	.190	cm^3/gm	Excluded volume for vapor phase
a_y	47.	Mbar (cm^3/mole)	Coefficient of attractive potential for vapor
θ	1.0	dimensionless	Join parameter
DELS	1.555×10^{-4}	Mbar-cm^3/mole-deg	Entropy of melting
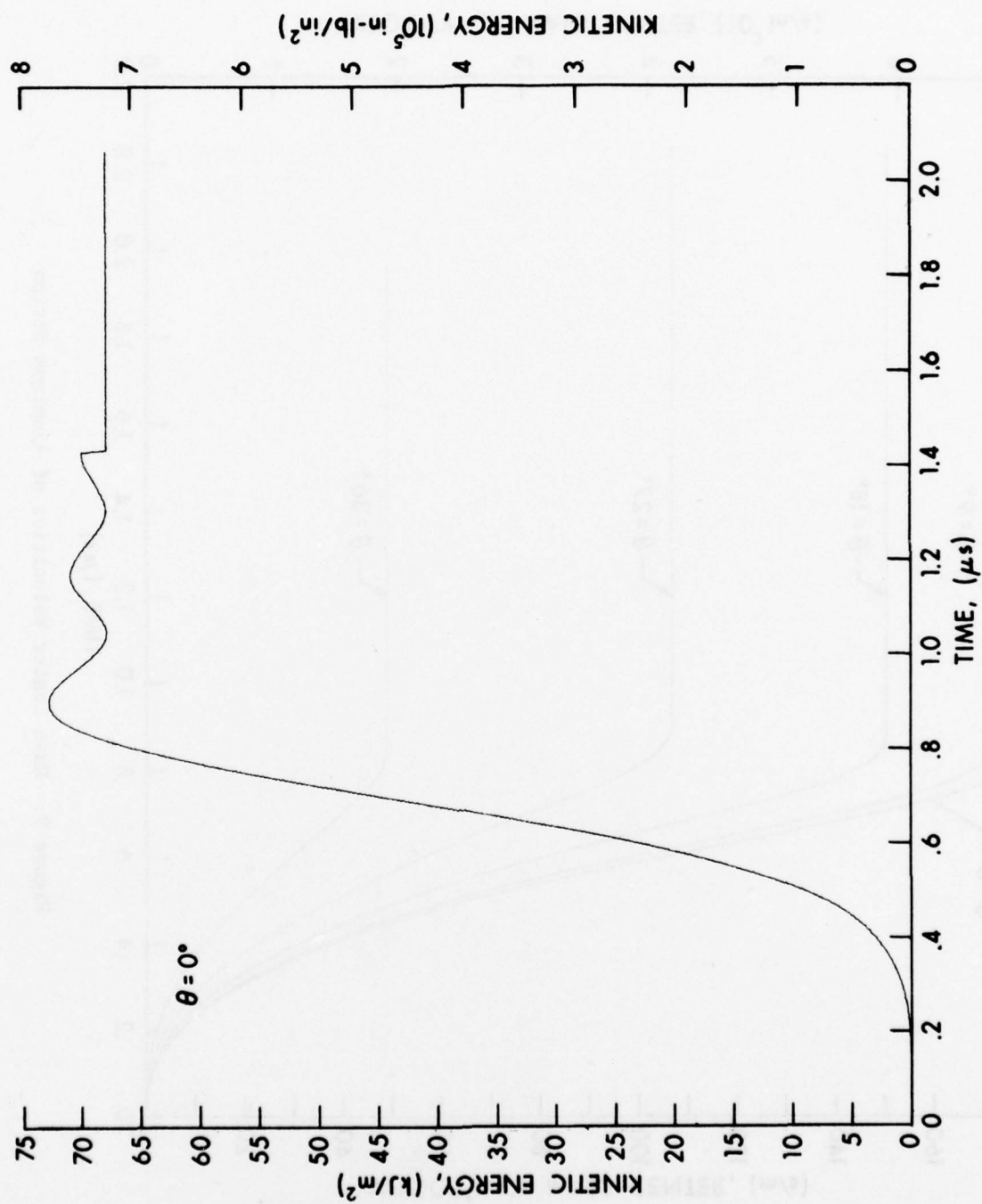
Figure 8. Kinetic Energy of Aluminum Strip

19
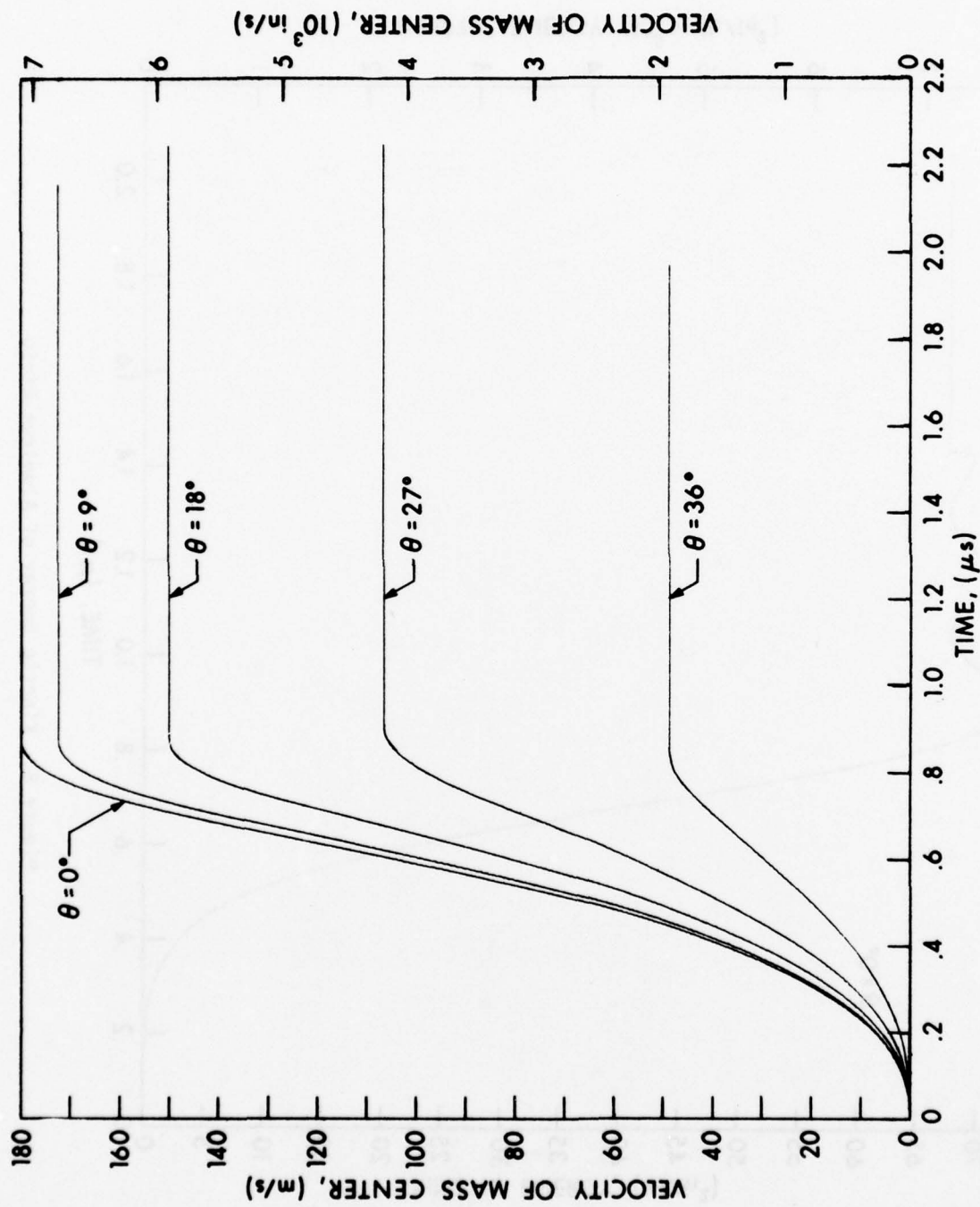
Figure 9. Mass Center Velocities of Aluminum Strips

20
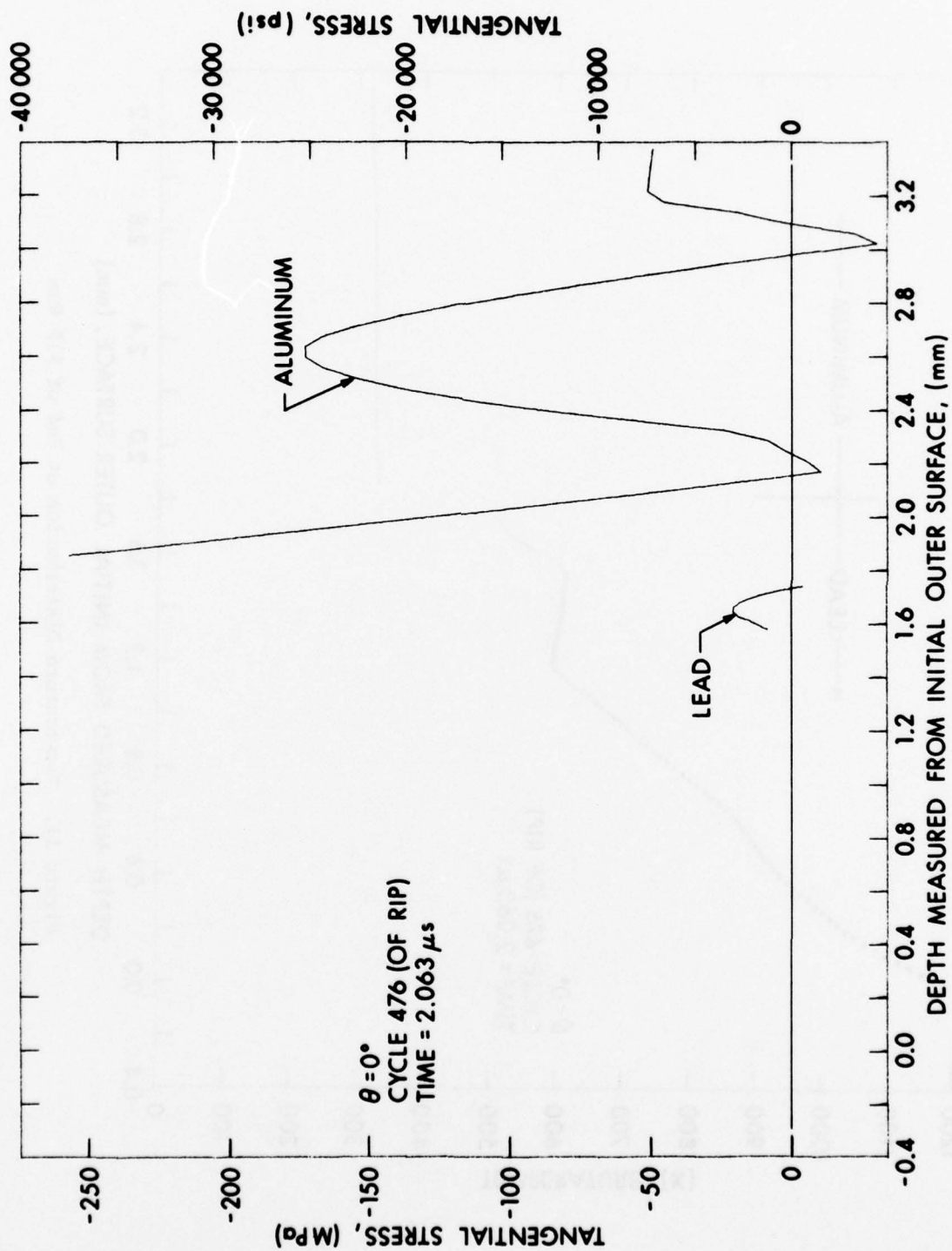
Figure 10. Residual Tangential Stresses at End of RIP Run

21
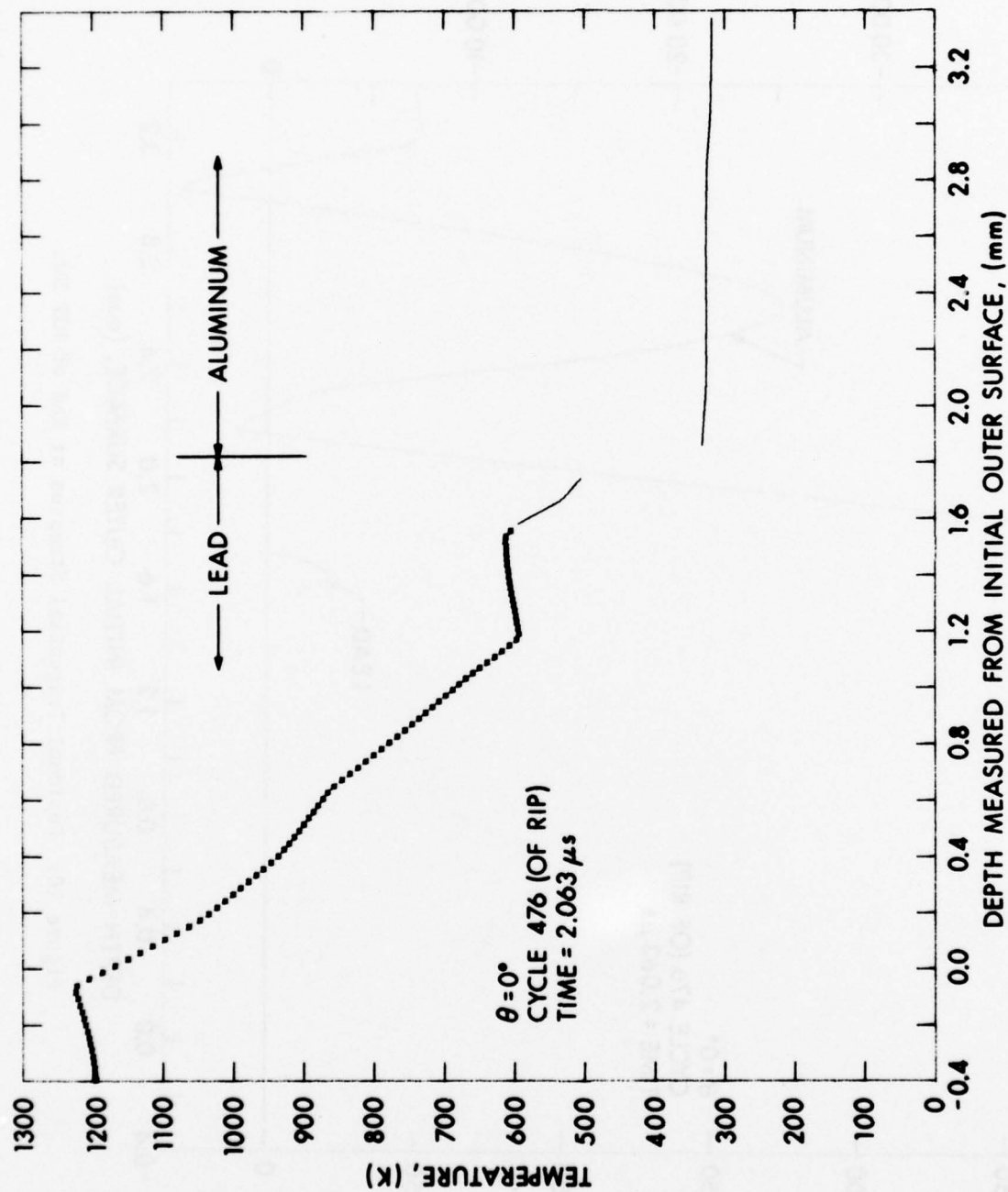
Figure 11. Temperature Distribution at End of RIP Run

The RIP code solutions also yield information concerning the thickness of solid lead remaining after electron beam deposition as a function of circumferential angle (see Figure 12). This variation of thickness appears to be in reasonable agreement with that of the recovered overlay. Precise thickness comparisons are not feasible since the overlay experienced stretching and additional thinning before rupturing. Also plotted in Figure 12 (to an arbitrary scale) is the circumferential variation of radial velocity of the aluminum cylinder which is to be transferred as an initial condition to the structural response analysis.
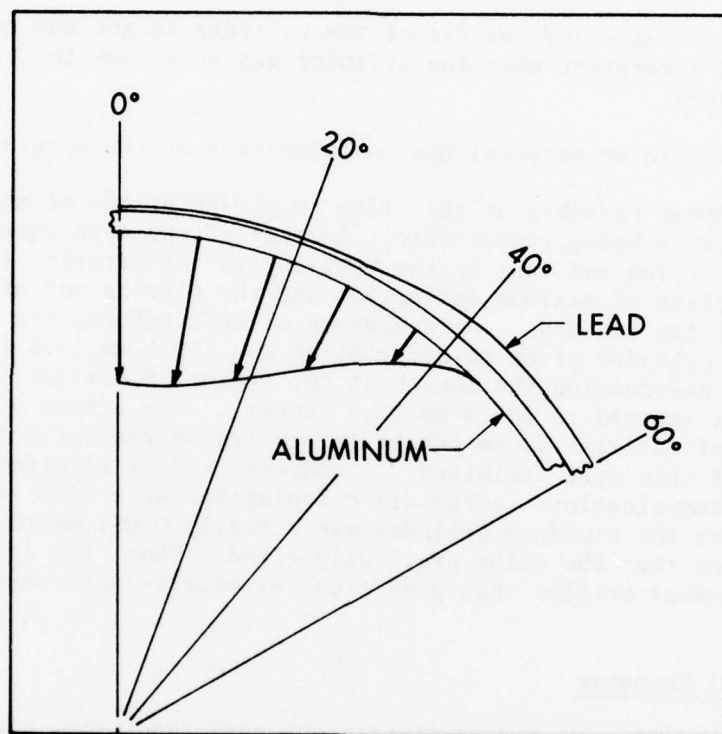
Figure 12. Thickness and Velocity Distributions

B. Caveats Concerning Imperfect Modeling

Before proceeding with consideration of response predictions it is appropriate to note those non-ideal aspects of the experimental procedure which will be ignored in the modeling but which may contribute to discrepancies between predictions and experimental data. By examination of the recovered lead overlay (see Figure 4) it may be inferred that the electron beam deposition was not completely uniform for the longitudinal direction of the cylinder and that the variation of intensity was not symmetric with respect to the mid-length of the cylinder. This effect is apparent in the deformed cylinder (Figure 3)

23

also, where the maximum deflection is located about 12.7 mm (0.5 inch) from the mid-cross section. Further, it is observed that the response pattern of the cylinder seems to be rotated about 12° with respect to the $\theta = 0°$ plane. There are several possible causes for this effect:

(a) The $\theta = 0°$ strain gage may not have been aligned with the incident beam.

(b) The incident beam axis may have been above or below the cylinder axis.

(c) The looseness of the fit of the cylinder in the end caps may have permitted a rotation when the cylinder was struck by the beam (pendulum effect).

(d) Geometric or material non-uniforunities of the specimen.

It does not appear possible at this time to pin-point one of these possible causes as being responsible. Another effect associated with the looseness of the end caps is the "pulling-in" of material in the longitudinal plane of maximum deflection and the flaring out of material which overlays the end caps. As a measure of this effect, the total length of the cylinder prior to deformation was 190.5 mm (7.5 inches), whereas after deformation the length at the region of maximum transverse deflection was reduced to 185.4 mm (7.3 inches). The effect of this "pulling-in" of material is to permit larger transverse deflections than would occur if this were inhibited. A converse effect resulted from an error in communication: after all calculations were completed it was discovered that the aluminum cylinder was actually 0.051 mm (0.002 inches) thicker than the value previously cited. Thus, the cylinder should be somewhat stiffer than predicted, especially with regard to flexure.

C. Structural Response

The structural response prediction was performed using the PETROS 3.5 code, the aluminum cylinder being modeled as having fixed ends and as being fabricated from an elastic, perfectly plastic material (see Figure 1) with a yield stress of 276.5 MPa (40100 psi) and a density of 2701 kg/m^3(0.0002528 lb sec^2/in^4). The lead overlay was ignored in this calculation since (a) it was not bonded to the aluminum cylinder and (b) high speed photography showed the overlay rapidly peeling away from the structural shell. The distributions of residual tangential stresses and the velocity distribution of Figure 12 were used as initial conditions for the response calculation, assuming that there was no longitudinal variation of these quantities.

The evolution of the final deformation pattern is illustrated in Figure 13. The grid defining the cylinder surface in the isometric views is the actual finite difference grid employed for the calculations. The
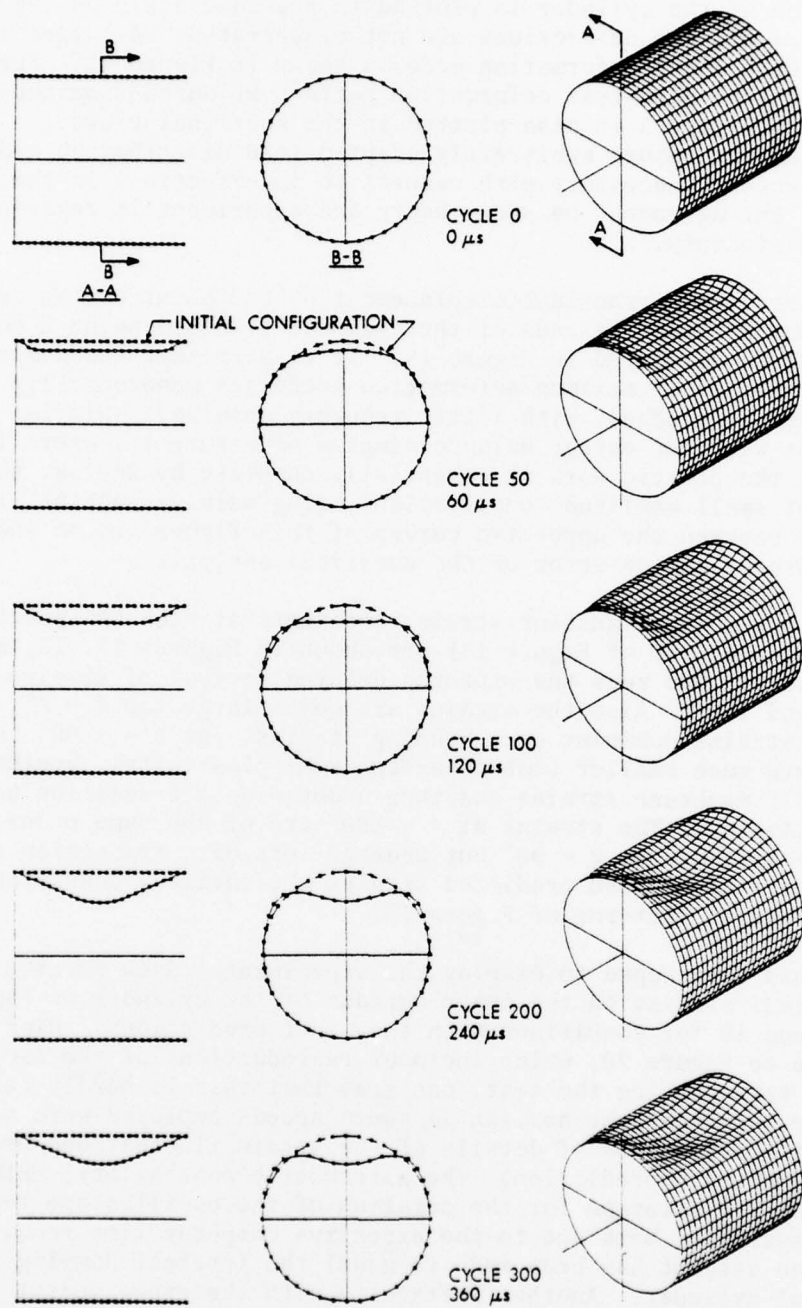
24

Figure 13. Transient Deformation Patterns of the Aluminum Cylinder

25

deformation of the cylinder is plotted to the same scale as the initial geometry; i.e., the deflections are not exaggerated. A larger view of the predicted final deformation mode is shown in Figure 14. For comparison, the post-test deformation pattern measured from the cylinder of Figure 3 is also plotted in the sectional views. Considering the rather arbitrarily adapted load distribution and the numerous caveats necessary with respect to imperfections in the modeling, the agreement between theory and experiment is regarded as quite satisfactory.

The predicted transient displacement of the point on the crown line midway between the ends of the cylinder (labeled point B on Figure 14) is displayed in Figure 15. It is seen that the deflection at this position of maximum deformation increases monotonically until the maximum is reached, with little recovery ensuing. This is consistent with the energy balance diagram of Figure 16, where it may be seen that the plastic work is essentially complete by 260 μs, the subsequent small amplitude oscillations being mainly elastic. The small gap between the upper two curves of this figure are an indication of the discretization error of the numerical analysis.

The predicted transient strain components at each 90° position (Points B, A & C, D of Figure 14) are shown in Figures 17, 18, and 19, respectively. One sees the expected delayed arrival of strains at $\theta = 90°$ and 180°. Also the strains are quite large for $\theta = 0°$, with membrane strains dominant over bending strains. At $\theta = \pm 90°$ the strains are much smaller (but entailing some plasticity), beginning as principally membrane strains and then undergoing a transition to mostly bending strains. The strains at $\theta = 180°$ are of the same order of magnitude as those at $\theta = 90°$ but undergo less of a transition to bending strains. These predicted strains are entirely consistent with the deformation patterns of Figure 13.

It had been hoped to display the experimental data for the longitudinal strains on the inner surface of the cylinder on Figures 17, 18, and 19 for comparison with the model predictions. However, by reference to Figure 20, which includes reproductions of the oscilloscope pictures taken during the test, one sees that this is hardly feasible. It may be seen that the horizontal sweep speeds employed were too slow to permit observations of details of the strain fluctuations provided by the PETROS 3.5 prediction. The alternative possibility, extending the PETROS 3.5 solution for the duration of the oscilloscope records is not desirable, both due to the excessive computer time required and because no attempt has been made to model the internal damping in the structural cylinder. Another difficulty with the experimental data concerns the location of zero for the vertical axis; this was initially set on the horizontal axis having tic marks but may have drifted somewhat before the electron beam pulse was activated. Further, no trace was recorded for gage A and both gages A and B were found to be disconnected after the test. It is believed that gage B failed very

26

POINT B

A

A

EXPERIMENTAL CONTOUR

B

B

A-A

B-B

A

B

C

D
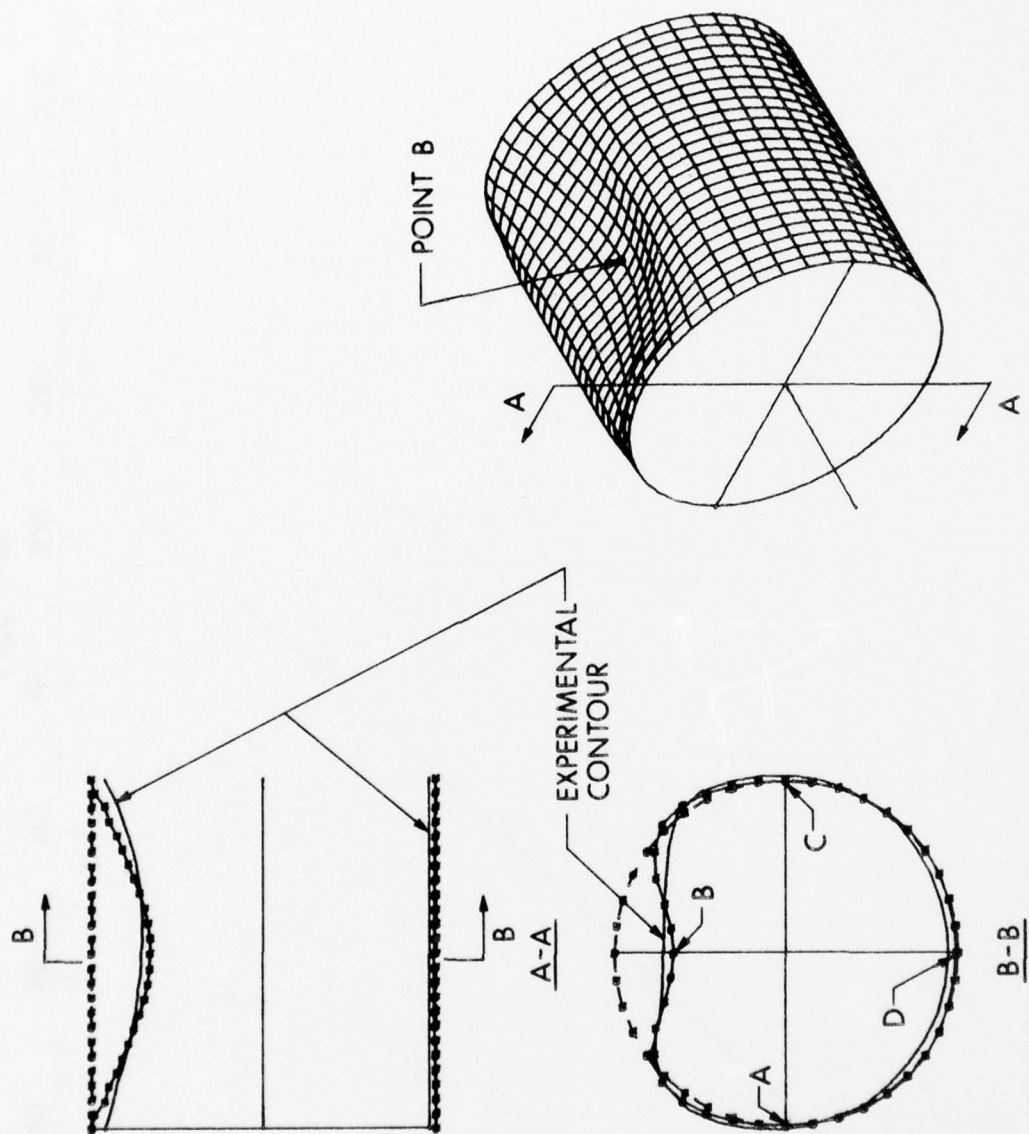
Figure 14. Comparison Between Experimental Data and PETROS 3.5 Predictions
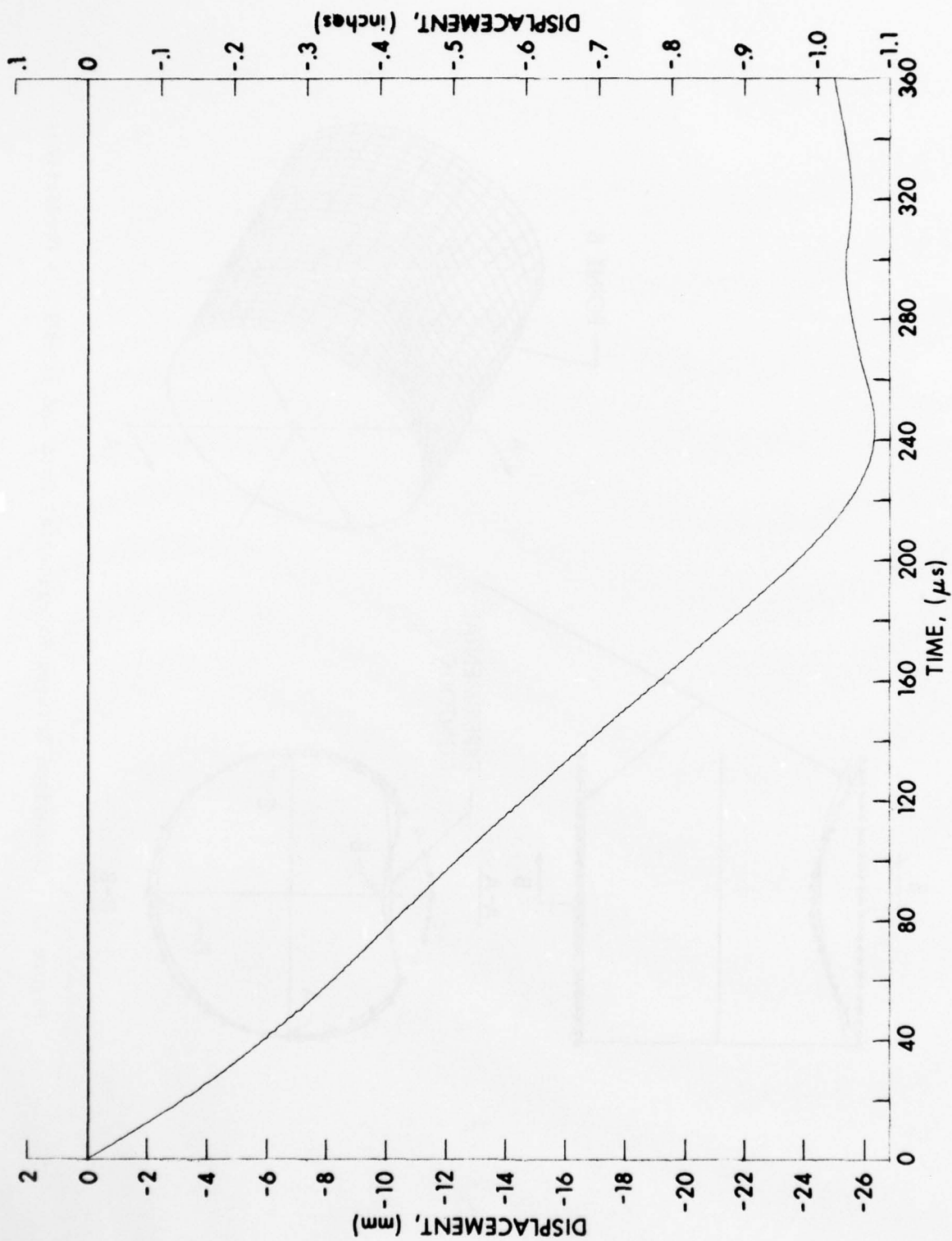
Figure 15. Displacement at Mid-Length, θ = 0°

28
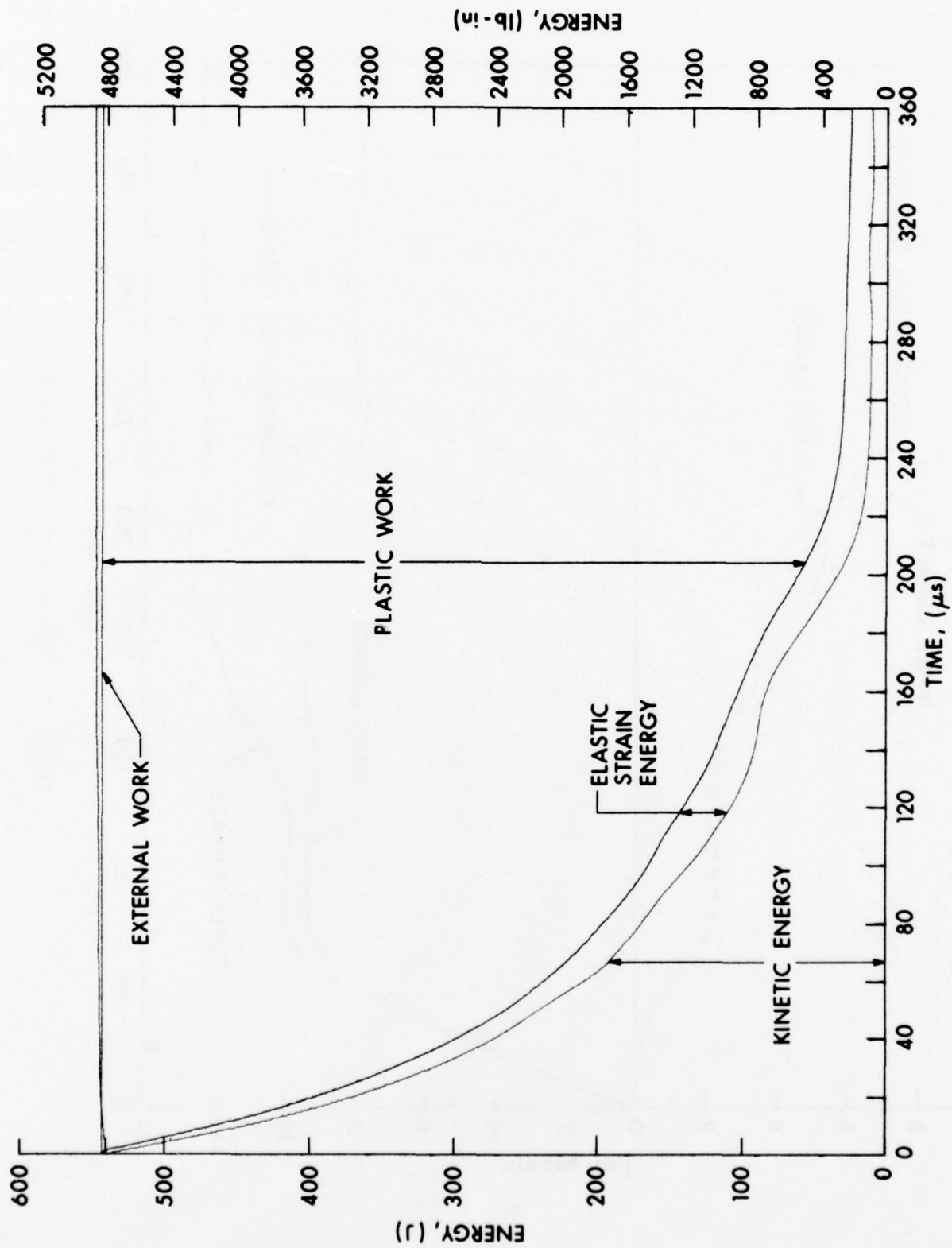
Figure 16. Energy Balance Diagram for Aluminum Cylinder Response

29
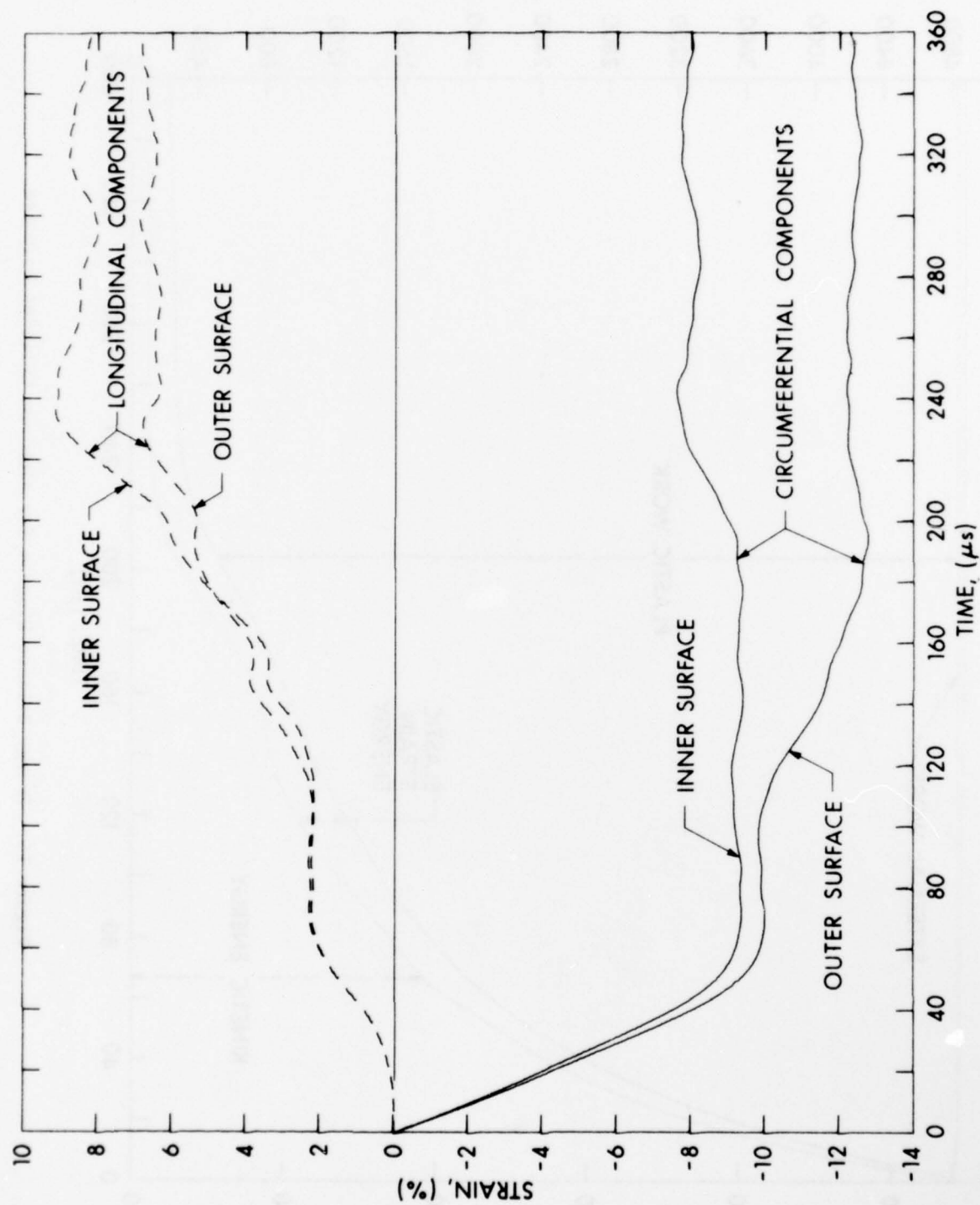
Figure 17. Strains at θ = 0° (Point B)

30
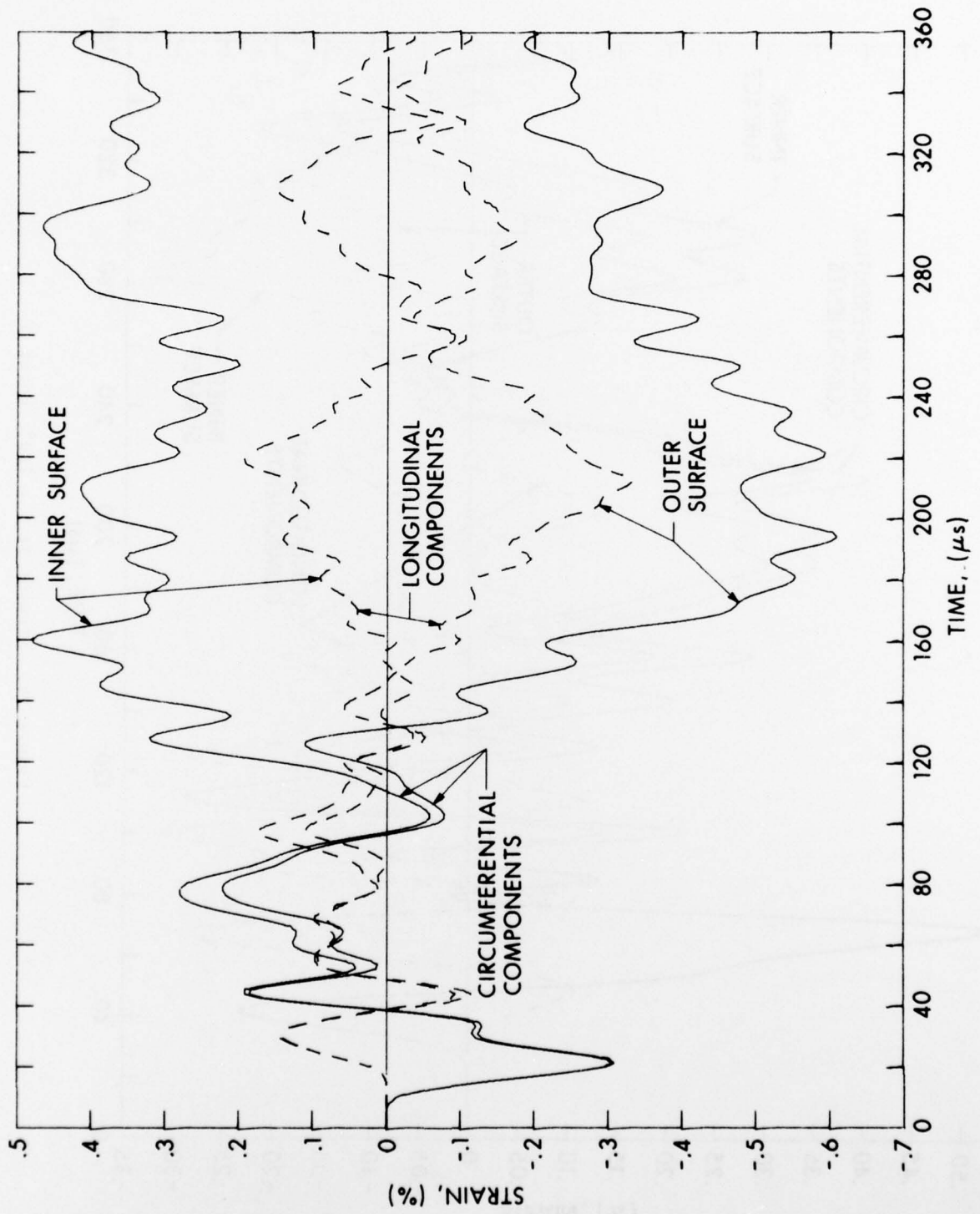
Figure 18.   Strains at $\theta = \pm 90°$ (Points A, C)

31
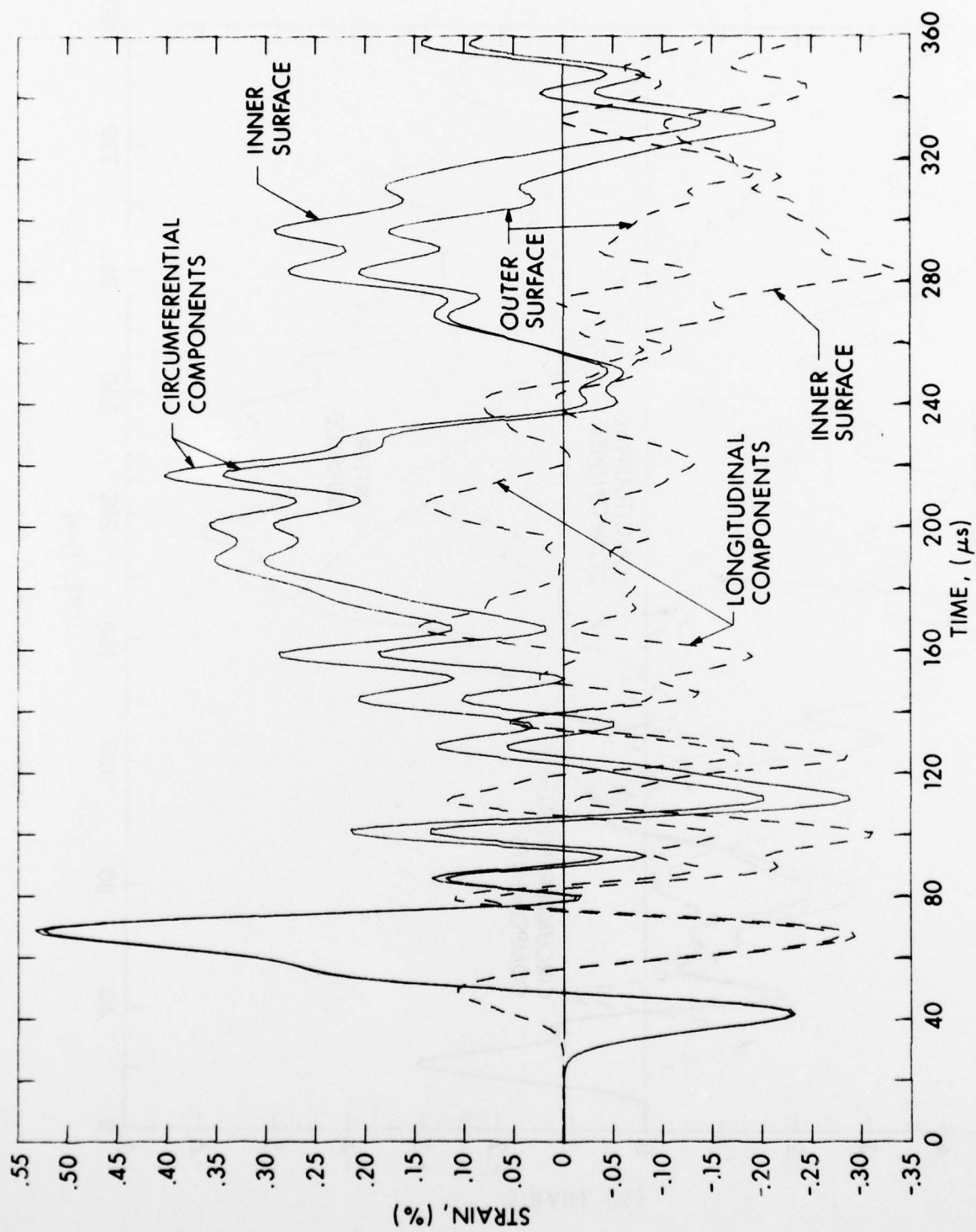
Figure 19. Strains at $\theta = 180°$ (Point D)

(a) POINT B (θ = 0°)

(b) POINT C (θ = 90°)
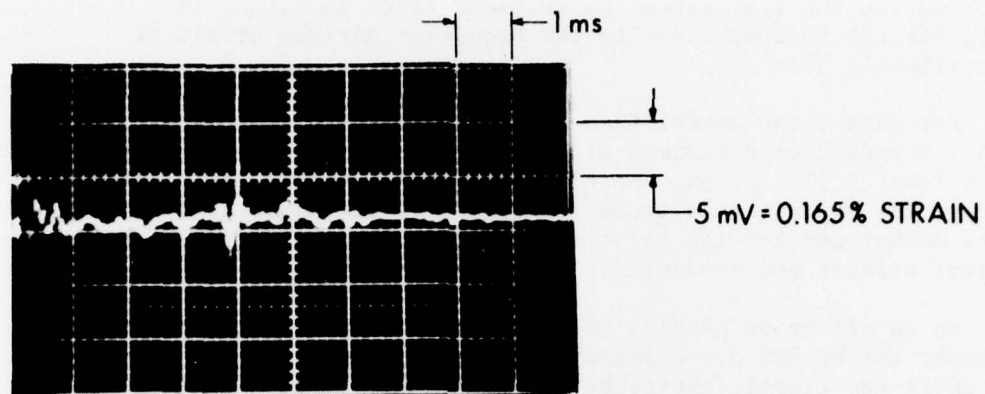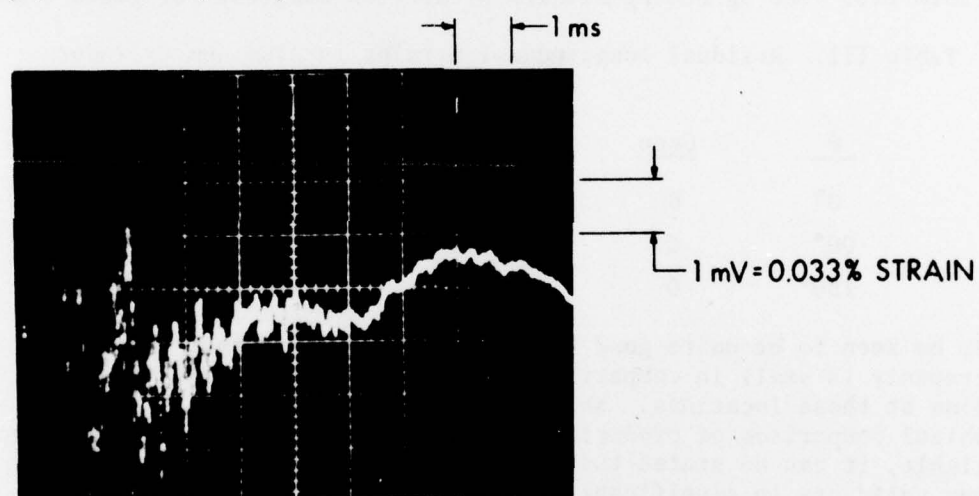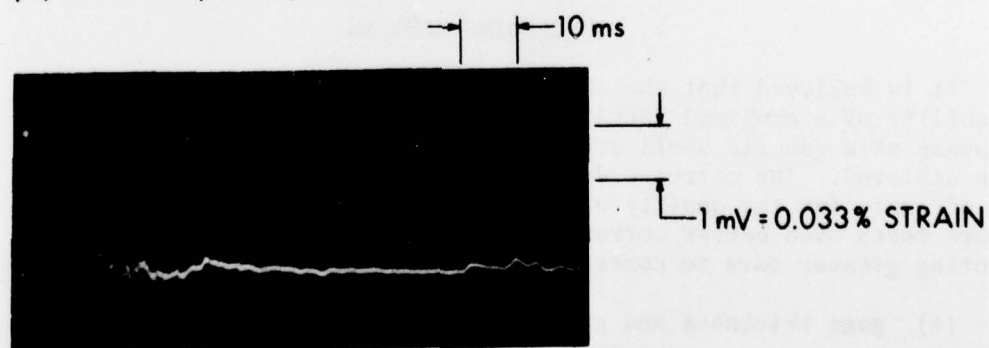
(c) POINT D (θ = 180°)

Figure 20.   Longitudinal Strain vs Time at Indicated Locations

33

early during the test since the recorded trace amplitude is insignificant in comparison to the predicted maximum strain of approximately 9%.

For gage C the correlation between theory and experiment is rather good: the predicted maximum strain is 0.2% while the experimental value is at least 0.17%, perhaps more if the trace went off scale. Unfortunately, the experimental trace for gage D is invisible against the dense background for the first seven milliseconds, during which the largest strains are predicted.

In an effort to predict the residual strains in the aluminum cylinder the PETROS 3.5 calculations were restarted with damping and run until the kinetic energy became negligibly small. These predicted residual strains are compared to the corresponding experimental values in Table III. The agreement between prediction and test for gages C and

Table III. Residual Longitudinal Strains in Aluminum Cylinder

| | | Longitudinal Strain | |
θ	Gage	Predicted	Experimental
0°	B	8.29%	invalid
90°	C	0.04%	0.01%
180°	D	-0.11%	-0.09%

D may be seen to be quite good when it is appreciated that the discrepancy is small in comparison to the magnitudes of the transient strains at these locations. While it is dissappointing that a graphical comparison of predicted and measured transient strains is not available, it can be stated that no experimental strain data which appear valid are in significant disagreement with predictions.

V. CONCLUDING REMARKS

It is believed that the objective of demonstrating the capability of a combined ZEBRA/RIP/PETROS 3.5 analysis to model the response of a generic shell structure to electron beam loading has been achieved. The correspondence between predictions and test data was adequate for the quality of experimental results available. In future tests even better correspondence should be attainable by devoting greater care to control or measurement of:

(a) gage thickness and geometrical imperfections of specimens

(b) material properties (including possible rate effects)

(c) boundary conditions (which can be readily modeled).

The performance of pre-test predictions should assist in the selection and adjustment of instrumentation and result in better quality experimental data.

As noted previously, the only obstacle to successful use of the AURORA facility in the electron beam mode as an x-ray loading simulator is the apparent absence of an analytical model relating the electron beam "free field" to the fluence distribution over the surface of the target; i.e., to the input to the ZEBRA calculations. This modeling gap was circumvented in the present investigation by an intuitively deduced circumferential distribution which must have been reasonably close to the physical distribution, judged by the success in predicting the deformation pattern of the target. However, for future more complex applications a satisfactory model for fluence distribution should be developed.

ACKNOWLEDGMENTS

DISTRIBUTION LIST

No. of Copies	Organization	No. of Copies	Organization
12	Commander Defense Documentation Center ATTN: DDC-TCA Cameron Station Alexandria, VA 22314	4	Director Defense Nuclear Agency ATTN: SPTL Tech Lib (2 cys) APSI (ARCHIVES) STSP Washington, DC 20305
1	Director Defense Advanced Research Projects Agency 1400 Wilson Boulevard Arlington, VA 22209	1	Commander Field Command Defense Nuclear Agency ATTN: Tech Lib, FCWS-SC Kirtland AFB, NM 87115
1	Director Weapons Systems Evaluation Group, ODDR&E ATTN: CPT Donald E. McCoy Washington, DC 20305	1	Chief Las Vegas Liaison Office Field Command TD, DNA P.O. Box 2702 ATTN: Document Control Las Vegas, NV 89104
1	Assistant to the Secretary of Defense (Atomic Energy) ATTN: Document Control Washington, DC 20301	1	DNA Information and Analysis Center TEMPO, General Electric Co. Center for Advanced Studies ATTN: DASIAC 816 State Street Santa Barbara, CA 93102
1	Office of Deputy Under Secretary of Defense for Research and Engineering (ET) Staff Specialist for Materials and Structures ATTN: Mr. Jerome Persh Room 3D1089, The Pentagon Washington, DC 20301	1	Director Defense Communications Agency ATTN: NMCSSC (Code 510) Washington, DC 20305
7	Director Defense Nuclear Agency ATTN: Mr. J. F. Moulton, SPAS Mr. D. Kohler, SPAS Dr. LaVier, STVL Cdr Alderson, RATN Mr. J. Farber, RAEV Dr. E. Sevin, SPSS Dr. M. C. Atkins, DDST Washington, DC 20305	2	Director Defense Intelligence Agency ATTN: DT-1C, Dr. J. Vorona DT-2 Washington, DC 20301
		3	Director Institute for Defense Analyses ATTN: Dr. J. Menkes Dr. J. Bengston Tech Info Ofc 400 Army-Navy Drive Arlington, VA 22202

DISTRIBUTION LIST

No. of Copies	Organization

2 Chairman
  Joint Chiefs of Staff
  ATTN: J-3, Operations
        J-5, Plans & Policy
            (R&D Division)
  Washington, DC 20301

1 Commander
  US Army Materiel Development
    and Readiness Command
  ATTN: DRCDMA-ST
  5001 Eisenhower Avenue
  Alexandria, VA 22333

1 Commander
  US Army Aviation Research
    and Development Command
  ATTN: DRSAV-E
  12th and Spruce Streets
  St. Louis, MO 63166

1 Director
  US Army Air Mobility Research
    and Development Laboratory
  Ames Research Center
  Moffett Field, CA 94035

1 Commander
  US Army Electronics Command
  ATTN: DRSEL-RD
  Fort Monmouth, NJ 07703

3 Commander
  US Army Missile Research
    and Development Command
  ATTN: DRDMI-R
        DRDMI-AOM, Library
        DRDMI-RSS, Mr. B. Cobb
  Redstone Arsenal, AL 35809

1 Commander
  US Army Tank Automotive
    Research and Development
    Command
  ATTN: DRDTA-RWL
  Warren, MI 48090

2 Commander
  US Army Mobility Equipment
    Research and Development
    Command
  ATTN: Tech Docu Cen, Bldg 315
        DRSME-RZT
  Fort Belvoir, VA 22060

1 Commander
  US Army Armament Materiel
      Readiness Command
  ATTN: DRSAR-LEP-L, Tech Lib
  Rock Island, IL 61299

4 Commander
  US Army Armament Research
    and Development Command
  ATTN: DRDAR-LC, Dr. J. Frasier
        DRDAR-LCF,
          Mr. G. Denitrack
        DRDAR-LCN, Mr. W. Benson
        DRDAR-LCN,
          Mr. P. Angelotti
  Dover, NJ 07801

1 Commander
  US Army Watervliet Arsenal
  Watervliet, NY 12189

38

DISTRIBUTION LIST

No. of Copies	Organization	No. of Copies	Organization
7	Commander US Army Harry Diamond Labs ATTN: DRXDO-TI Mr. R. Bostak Mr. P. A. Caldwell Dr. W. Carter Mr. J. Corrigan Mr. E. J. Gaul Mr. S. Graybill 2800 Powder Mill Road Adelphi, MD 20783	1	Commander US Army Foreign Science and Technology Center ATTN: Rsch & Data Branch Federal Office Building 220 - 7th Street, NE Charlottesville, VA 22901
7	Commander US Army Harry Diamond Labs ATTN: Mr. J. Gwaltney Mr. T. R. Oldham Dr. R. Oswald Dr. D. Schallhorn Mr. W. D. Scharf Mr. G. L. *Skillington* Mr. F. N. Wimenitz 2800 Powder Mill Road Adelphi, MD 20783	2	Commander US Army Nuclear Agency 7500 Backlick Road, Bldg 2073 Springfield, VA 22150
		1	Commander US Army TRADOC Systems Analysis Activity ATTN: ATAA-SL, Tech Lib White Sands Missile Range NM 88002
3	Commander US Army Materials and Mechanics Research Center ATTN: DRXMR-ATL DRXMR-ED Mr. R. Shea DRXRD, J. Dignam Watertown, MA 02172	1	Interservice Nuclear Weapons School ATTN: Technical Library Kirtland AFB, NM 87115
1	Commander US Army Natick Research and Development Command ATTN: DRXRE, Dr. D. Sieling Natick, MA 01762	1	Director DARCOM Field Safety Activity ATTN: DRXOS-ES Charlestown, IN 47111
		1	Director DARCOM, ITC ATTN: Dr. Chiang Red River Depot Texarkana, TX 75501
		1	Director US Army Ballistic Missile Defense Program Office ATTN: J. Shea 5001 Eisenhower Avenue Alexandria, VA 22333

DISTRIBUTION LIST

No. of Copies	Organization	No. of Copies	Organization

6	Director
	US Army Ballistic Missile
	  Defense Advanced Technology
	  Center
	ATTN: M. Whitfield
	       J. Davidson
	       M. Capps
	       N. J. Hurst
	       J. G. Bauxbaum
	       J. Veeneman
	P.O. Box 1500, West Station
	Huntsville, AL 35807
		2	Director
			Joint Strategic Target
			  Planning Staff
			ATTN: JLTW
			       JPTP
			Offutt AFB
			Omaha, NB 68113

1	Director
	US Army Engineer School
	Fort Belvoir, VA 22060
		4	Chief of Naval Operations
			ATTN: OP-03EG
			       OP-97
			       OP-754
			       OP-985FZ
			Department of the Navy
			Washington, DC 20350

1	HQDA (DAMA-AR; NCL Div) Washington, DC 20310	1	Assistant Secretary of the Navy (Research & Development) Navy Department Washington, DC 20350
1	Commander US Army Research Office P.O. Box 12211 Research Triangle Park NC 27709	1	Chief of Naval Material ATTN: Code 418, Dr. T. Quinn Navy Department Arlington, VA 22217

1	Director
	US Army Engineer Waterways
	  Experiment Station
	P.O. Box 631
	Vicksburg, MS 39180
		4	Commander
			David W. Taylor Naval Ship
			  Research & Development Center
			ATTN: Dr. W. W. Murray, Code 17
			       Mr. R. Jones, Code 1725
			       Dr. G. Everstine, Code 1844
			       Dr. B. Whang, Code 174.4
			Bethesda, MD 20084

1	US Army Eng Div ATTN: Mr. Char P.O. Box 1600 Huntsville, AL 35809	2	Commander US Naval Surface Weapons Center ATTN: Mr. J. C. Talley Dr. W. Soper Dahlgren, VA 22448
1	US Army Corps of Engineers Huntsville Division ATTN: Dick Bradshaw HNDED-SR P.O. Box 1600, West Station Huntsville, AL 35807		

DISTRIBUTION LIST

No. of Copies	Organization	No. of Copies	Organization
4	Commander US Naval Surface Weapons Center ATTN: Dr. Leon Schindel Dr. Victor Dawson Dr. P. Huang Code 121, Navy Nuclear Programs Office Silver Spring, MD 20910	2	Superintendent US Naval Postgraduate School ATTN: Tech Reports Section Code 57, Prof R. Ball Monterey, CA 93940
1	Commander Naval Surface Weapons Center ATTN: Code 241 (Mr. Proctor) Silver Spring, MD 20910	1	HQ USAF (AFNIE-CA) Washington, DC 20330
		4	HQ USAF (AFRDQ; AFRDOSM; AFRDPM; AFRD) Washington, DC 20330
1	Commander US Naval Weapons Center ATTN: Code 6031 Dr. W. Stronge China Lake, CA 93555	1	AFSC (DSCPSL) Andrews AFB Washington, DC 20331
1	Commander US Naval Ship Research and Development Center Facility ATTN: Mr. Lowell T. Butt Underwater Explosions Research Division Portsmouth, VA 23709	2	AFATL (ATRD, R. Brandt) Eglin AFB, FL 32542
		1	ADTC (ADBPS-12) Eglin AFB, FL 32542
		1	USAFTAWC (OA) Eglin AFB, FL 32542
1	Commander US Naval Weapons Evaluation Facility ATTN: Document Control Kirtland AFB Albuquerque, NM 87117	3	AFWL (WLA; WLD; WLRP, LTC H. C. McClammy) Kirtland AFB, NM 87117
		4	AFWL (SYT, MAJ W. A. Whitaker; SRR; SUL; SR) Kirtland AFB, NM 87117
1	Commander Naval Civil Engineering Lab ATTN: J. Tancreto Port Hueneme, CA 93041	2	AFWL (J. Place; D. Newlander, DYV) Kirtalnd AFB, NM 87117
		1	AFFDL/FBE (Dr. R. M. Bader) Wright-Patterson AFB, OH 45433
1	Commander US Naval Research Laboratory ATTN: Code 2027, Tech Lib Washington, DC 20375	4	AFML (MAMD, Dr. T. Nicholas; MAS; MANC, Mr. D. Schmidt; MAX, Dr. A. M. Lovelace) Wright-Patterson AFB, OH 45433

41

DISTRIBUTION LIST

No. of Copies	Organization	No. of Copies	Organization
2	FTD (TDPTN; TDFBD, J. D. Pumphrey) Wright-Patterson AFB, OH 45433	1	Director Los Alamos Scientific Lab ATTN: Dr. J. Taylor P.O. Box 1663 Los Alamos, NM 87544
1	Headquarters Energy Research and Development Administration Department of Military Applications Washington, DC 20545	7	Sandia Laboratories ATTN: Infor Distr Division Dr. W. Herrmann Dr. S. W. Key Mr. R. D. Krieg Dr. A. Chabai Mr. L. Posey Dr. W. A. von Riesemann Albuquerque, NM 87115
2	Headquarters National Aeronautics and Space Administration ATTN: Mr. J. Enders, Code RAO Mr. K. Strass, Code RY Washington, DC 20546	1	Director ATTN: J. Nall P.O. Box 1925 Washington, DC 20505
2	National Aeronautics and Space Administration Aerospace Safety Research and Data Institute ATTN: Mr. S. Weiss Mail Stop 6-2 Mr. R. Kemp Mail Stop 6-2 Lewis Research Center Cleveland, OH 44135	1	National Academy of Sciences ATTN: Mr. D. G. Groves 2101 Constitution Avenue, NW Washington, DC 20418
1	Director NASA Scientific and Technical Information Facility ATTN: SAK/DL P.O. Box 8757 Baltimore/Washington International Airport, MD 21240	1	Aeronautical Research Associates of Princeton, Inc. ATTN: Dr. C. Donaldson 20 Washington Road Princeton, NJ 08540
		1	Aerospace Corporation ATTN: Dr. Harris Mayer P.O. Box 95085 Los Angeles, CA 90045
1	Director Lawrence Livermore Laboratory Technical Information Division P.O. Box 808 Livermore, CA 94550	2	AVCO Corporation Structures and Mechanics Dept ATTN: Dr. William Broding Mr. J. Gilmore Wilmington, MA 01887

42

DISTRIBUTION LIST

No. of Copies	Organization
2	Bell Aerosystems Company ATTN: Dr. W. H. Dukes Mr. J. Padlog P.O. Box 1 Buffalo, NY 14205
1	Bell Telephone Labs, Inc. ATTN: Mr. M. F. Stevens Mountain Avenue Murray Hill, NJ 07971

2	The Boeing Company
	Aerospace Group
	ATTN: Dr. Peter Grafton
	      Dr. D. Strome
	         Mail Stop 8C-68
	Seattle, WA 98124

1	The Boeing Company ATTN: B. Lempriere P.O. Box 3707 Seattle, WA 98124
1	Effects Technology ATTN: M. Rosen 5383 Holister Avenue Santa Barbara, CA 93111
1	J. G. Engineering Research Associates 3831 Menlo Drive Baltimore, MD 21215
1	Kaman AviDyne ATTN: Dr. N. P. Hobbs Mr. S. Criscione Northwest Industrial Park 83 Second Avenue Burlington, MA 01803

3	Kaman Sciences Corporation
	ATTN: Dr. F. H. Shelton
	      Dr. D. Sachs
	      Dr. R. Keefe
	1500 Garden of the Gods Road
	Colorado Springs, CO 80907

No. of Copies	Organization
1	Kaman Sciences Corporation P.O. Box 7463 ATTN: John Oscarson Colorado Springs, CO 80933
1	Knolls Atomic Power Lab ATTN: Dr. R. A. Powell Schenectady, NY 12309

3	Lockheed Missiles and
	   Space Company, Inc.
	Division of Lockheed Aircraft
	   Corporation
	ATTN: R. Robertson
	      C. Vivian
	      Dick Walz
	P.O. Box 504
	Sunnyvale, CA 94088

3	Lockheed Missiles and
	   Space Company
	Aerospace Research Laboratory
	ATTN: Dr. Bushnell
	      Dr. R. Hartung
	      Mr. P. Underwood
	3251 Hanover Street
	Palo Alto, CA 94301

1	Martin Marietta Laboratories ATTN: Mr. R. Goldman 1450 S. Rolling Road Baltimore, MD 21227
1	Martin Marietta Laboratories ATTN: Mr. J. I. Bacile Orlando, FL 32805
1	McDonnell Douglas Astronautics Western Division ATTN: Dr. Les Cohen 5301 Bolsa Avenue Huntington Beach, CA 92647

DISTRIBUTION LIST

No. of Copies	Organization	No. of Copies	Organization
2	Physics International ATTN: Dr. G. Richard Fowles Mr. J. Shea San Leandro, CA 94577	1	Ohio State University Department of Engineering Mechanics ATTN: Prof K. K. Stevens Columbus, OH 43210
1	R&D Associates ATTN: Dr. Albert L. Latter P.O. Box 9695 Marina del Rey, CA 90291	1	Science Applications, Inc. ATTN: Olin Nance P.O. Box 1620 La Jolla, CA 92037
1	Simulation Physics Inc. ATTN: Mr. R. Little Patriots Park Bedford, MA 01730	3	Southwest Research Institute ATTN: Dr. H. N. Abramson Dr. W. E. Baker Dr. U. S. Lindholm 8500 Culebra Road San Antonio, TX 78228
1	Systems, Science and Software ATTN: Dr. J. K. Dienes P.O. Box 1620 La Jolla, CA 92037	1	Stanford Research Institute ATTN: Dr. W. Reuland 306 Wynn Drive, NW Huntsville, AL 35805
2	Battelle Columbus Laboratories ATTN: Dr. L. E. Hulbert Mr. J. E. Backofen, Jr. 505 King Avenue Columbus, OH 43201	1	Stanford University Department of Aeronautics and Astronautics ATTN: Prof C. R. Steele Stanford, CA 94305
1	Brown University Division of Engineering ATTN: Prof R. Clifton Providence, RI 01912	1	Stanford Research Institute 333 Ravenswood Avenue ATTN: Dr. H. Lindberg Menlo Park, CA 94025
1	Massachusetts Institute of Technology Aeroelastic and Structures Research Laboratory ATTN: Dr. E. A. Witmer Cambridge, MA 02139	1	Texas A & M University Department of Aerospace Engineering ATTN: Dr. Walter Haisler College Station, TX 77843
1	Massachusetts Institute of Technology Department of Ocean Engineering ATTN: Prof Norman Jones Cambridge, MA 02139	1	University of Alabama ATTN: Dr. T. L. Cost P.O. Box 2908 University, AL 35486

44

DISTRIBUTION LIST

No. of
Copies   Organization

   1   University of Delaware
       Department of Mechanical and
           Aerospace Engineering
       ATTN: Prof J. R. Vinson
       Newark, DE 19711

   1   The City College of the
           University of New York
       Department of Mechanical
           Engineering
       ATTN: Prof S. B. Menkes
       New York, NY 10031

Aberdeen Proving Ground

       Marine Corps Ln Ofc
       Dir, USAMSAA
          ATTN: Dr. J. Sperrazza
                 Mr. R. Norman, GWD